Probing dark-axionlike particle portals at future e^+e^- colliders

Sanjoy Biswas,[1,*] Anirban Chatterjee,[1,†] Emidio Gabrielli,[2,3,4,‡] and Barbara Mele[5,§]

[1]*Ramakrishna Mission Vivekananda Educational and Research Institute, Belur Math, Howrah 711202, India*

[2]*Physics Department, Theoretical Section, University of Trieste, Strada Costiera 11, I-34151 Trieste, and INFN, Sezione di Trieste, Via Valerio 2, I-34127 Trieste, Italy*

[3]*NICPB, Ravala 10, 10143 Tallinn, Estonia*

[4]*IFPU—Institute for Fundamental Physics of the Universe, Via Beirut 2, 34151 Trieste, Italy*

[5]*INFN, Sezione di Roma, P. le A. Moro 2, I-00185 Rome, Italy*

(Received 14 July 2019; published 24 December 2019)

We study portal interactions connecting visible and dark sectors, and involving local interactions of a photon, a dark photon and a axionlike particle (ALP) at future e^+e^- colliders. These interactions, mediated by higher-dimensional effective operators, may arise at one loop by kinetic mixing between dark and ordinary photons, or, for massless dark photons, by direct short-distance contributions. We explore these portal interactions for a heavy ALP with masses between about 10 and 230 GeV, and for a massless dark photon, by investigating the sensitivity of the production $e^+e^- \to \gamma\gamma\bar{\gamma}$ to the effective couplings, where the dark photon $\bar{\gamma}$ gives rise to missing momentum in the final state. We will show how an appropriate choice of missing-energy and missing-mass cuts can optimize the signal to standard-model background ratio. Exclusion regions for the effective photon-dark-photon-ALP couplings versus the ALP mass are worked out for a few representative values of the collision energy and integrated luminosity, as presently envisaged by future e^+e^- projects.

DOI: 10.1103/PhysRevD.100.115040

I. INTRODUCTION

The persistent global consistency of the Standard Model (SM) predictions against the data collected so far at the CERN Large Hadron Collider (LHC) is radically changing our perspective on the origin of possible new physics beyond the SM, and on its characteristic energy scale. This is also supported by the Higgs boson discovery [1], which is in good agreement with SM expectations [2,3]. On the other hand, the growing evidences for dark matter (DM) [4] and the lack of suitable DM candidates in the SM framework are strengthening the possibility of the existence of physics beyond the SM, provided DM does not have a purely gravitational origin, as in the case of primordial black holes. A proper new physics model should be able to explain the correct dark-matter relic abundance and other experimental constraints coming from the direct and indirect searches for DM, while keeping itself well decoupled from ordinary matter in order to escape present TeV-range constraints in the LHC searches.

The present picture can motivate the idea that the new physics responsible for DM might reside in a hidden or dark sector (DS), the latter consisting of new particles which are singlets under the SM gauge interactions. The DS can eventually interact with the SM via some portal-type interactions, mediated by heavy messengers which can communicate tree-level interactions between the SM and the DS fields [5]. This mechanism can give rise to low-energy effective interactions between SM and DS particles induced by higher-dimensional operators, the latter being suppressed by the characteristic scale of the messenger fields. Then, a quite heavy messenger sector might naturally explain why the new physics, and in particular the DM sector, is still escaping all direct and indirect searches [5].

A DS might contain a light or ultralight subsector. It might also be charged under its own long-distance interactions, in complete agreement with cosmological and astrophysical observations. Long-range forces mediated by a massless dark photon, corresponding to an exact $U(1)_D$ gauge symmetry in the DS, might also have a role in this picture. A DS scenario of the latter kind, which aims to solve the hierarchy puzzle of the SM Yukawa couplings, also providing natural DM candidates, has been recently

*sanjoy.biswas@rkmvu.ac.in
†anirban.chatterjee@rkmvu.ac.in
‡emidio.gabrielli@cern.ch
§barbara.mele@roma1.infn.it

proposed in [6,7], implying a possible deep connection between the origin of flavor and the DM interpretation.

Dark-photon scenarios (both in the massive and massless cases) have been extensively considered in the literature in new-physics extensions of the SM gauge group [5,8]. They have also been investigated in cosmology and astrophysics [9–16], mainly for improving models' predictions.

In collider physics, most of present dark-photon searches focus on massive dark photons, where the broken $U(1)_D$ gauge field naturally develops by kinetic mixing a tree-level (millicharged) interaction with ordinary charged matter [8]. However, a massless dark photon can behave in a radically different way with respect to a massive one. Indeed, the kinetic mixing among the ordinary photon and a massless dark photon can be rotated away, restricting dark-photon interactions with ordinary matter to higher-dimensional operators [8]. Most of the present astrophysical and laboratory constraints applying to massive dark photons can be evaded in the massless case, allowing for potentially large $U(1)_D$ couplings in the DS [13].

The DS could also contain the so-called axionlike particles (ALPs), a, loosely referring to neutral light (or ultralight) scalar (or pseudoscalar) particles. These particles can be present in SM extensions motivated by the solution to the strong charge-parity (CP) symmetry problem (in which case the ALP is a QCD axion [17]) or can be pseudo-Nambu-Goldstone bosons corresponding to spontaneously broken continuous symmetries, either in the visible or in the DS, or a moduli field in string models [18–21].

In the literature, the phenomenological aspects, including collider search of ALPs, have been extensively studied [22–28]. Most of these studies focus on the ALP effective coupling to photons and/or gluons via the usual $aF^{\mu\nu}\tilde{F}_{\mu\nu}$ and $aG^{\mu\nu}\tilde{G}_{\mu\nu}$ types of interaction, involving the photon and gluon field-strength tensors, respectively. In a possible theory UV completion, this kind of effective interactions could result (at one loop) from integrating out some heavy messenger fields connecting the dark and the observable sectors. Then the effective scale could be identified with the typical mass of the messengers running in the loop, properly rescaled by the product of internal couplings and loop factor suppressions.

While fixed-target experiments [29–31] and B factories [32] are particularly useful for searching new weakly coupled particles[1] like ALPs in the MeV-GeV range, high-energy colliders are more effective for constraining ALP masses above a few GeVs. Collider investigations carried out so far in this context, involving the aforementioned dimension-five operators, mostly focused on triphoton and/or monophoton+missing-energy signatures (depending on the ALP stability at the detector length scale) in the context of past and future e^+e^- collider experiments as well as of (HL-)LHC experiments [22,23,25–28].

Motivated by the above scenarios, we analyze a different type of portal interactions, that is dark-ALP portals which connect the visible sector and the DS via a higher-dimensional effective operator $aF^{\mu\nu}\tilde{\bar{F}}_{\mu\nu}$, involving a photon γ, a dark photon $\bar{\gamma}$, and an ALP a, being $\bar{F}_{\mu\nu}$ the dark-photon field strength. The $a\gamma\bar{\gamma}$ interaction can arise from the usual ALP coupling with photons, $aF^{\mu\nu}\tilde{F}_{\mu\nu}$, after rotating away the kinetic mixing in the photon dark-photon sector, or can directly be induced at one loop by short-distance effects, after integrating out some heavy messenger fields. The same kind of interactions has been considered in the context of various low-energy constraints in [35–37].

We are now going to focus on a massive ALP scenario, with the a mass M_a in the range of $10\ \text{GeV} \lesssim M_a \lesssim 230\ \text{GeV}$, and a massless dark photon. Indeed, the new effective operator not only provides a rich phenomenology in the context of astrophysical and cosmological observations, including the possibility of low-energy observations, but also opens up new ALP search strategies at collider experiments. In particular, we propose to look at the diphoton plus missing-energy channel $e^+e^- \to \gamma\gamma\bar{\gamma}$ with the aim to probe both the $aF^{\mu\nu}\tilde{F}_{\mu\nu}$ and $aF^{\mu\nu}\tilde{\bar{F}}_{\mu\nu}$ types of effective operators, in the context of future e^+e^- collider experiments. As we are going to illustrate through various kinematical distributions, that the diphoton plus missing-energy channel has distinctive kinematical features, thanks to the presence of a massless *invisible* dark photon, which will be helpful to efficiently separate the corresponding signal from the SM background by adopting various unconventional kinematic observables. In particular, we find that requiring an almost vanishing missing mass in the final state is most effective in separating the SM background. Moreover, the diphoton plus missing-energy channel has a better signal-to-background ratio compared to the conventional triphoton channel, even before imposing any hard cut on the final state objects.

While in the following we will assume new interactions involving a *pseudoscalar* ALP coupling, our results can be easily generalized for a neutral *scalar* particle.

The present search can be of relevance for the various e^+e^- collider projects that are presently under discussion, in particular for the linear colliders ILC [38], and CLIC [39], and for the circular options FCC-ee [40,41] and CEPC [42]. We will assume as reference for the collision center-of-mass (c.m.) energies, and integrated luminosities, the ones corresponding to the FCC-ee staging [43]. A straightforward projection for the setup corresponding to a different machine can be done in most cases.

We have organized the present paper in the following way. In the next section, we discuss the theoretical framework under consideration and various constraints

[1]Fixed target and beam dump experiments are also relevant for dark-photon searches as well. For details of experimental searches for dark photons, see [30,33,34].

relevant for the present study. In Sec. III, after presenting the LEP data implications on the present model, we suggest a new collider search strategy and corresponding event selection criteria at future e^+e^- colliders. Section IV contains the results of our analyses. Finally, our conclusions are reported in Sec. V.

II. THEORETICAL FRAMEWORK

A portal interaction connecting the dark sector and the visible sector can be parametrized in the following way:

$$\mathcal{L}_{\rm eff} = \frac{C_{a\gamma\gamma}}{\Lambda} a F^{\mu\nu}\tilde{F}_{\mu\nu} + 2\frac{C_{a\gamma\bar{\gamma}}}{\Lambda} a F^{\mu\nu}\tilde{\bar{F}}_{\mu\nu}, \qquad (1)$$

where $F^{\mu\nu}$ and $\bar{F}_{\mu\nu}$ are, respectively, the field strength of the photon γ and the dark photon $\bar{\gamma}$, a is the ALP field, $C_{a\gamma\bar{\gamma},a\gamma\bar{\gamma}}$ are dimensionless couplings, and Λ is some high energy scale[2] [35]. In principle, one could also add a term of the form $\frac{C_{a\bar{\gamma}\bar{\gamma}}}{\Lambda} a \bar{F}^{\mu\nu}\tilde{\bar{F}}_{\mu\nu}$ which might be present as well if one considers a specific UV completion of the low energy theory. The presence of such a coupling not only would reduce the branching ratio of the ALP decays $a \to \gamma\bar{\gamma}, \gamma\gamma$ by modifying the total decay width, but would also give an extra contribution to the diphoton plus missing-energy final state (at higher orders in perturbation theory) *via* the channel $e^+e^- \to \gamma\gamma^* \to \gamma\gamma a \to \gamma\gamma\bar{\gamma}\bar{\gamma}$. The event characteristics of the latter process would be similar to that of the SM background $e^+e^- \to \gamma\gamma\bar{\nu}\nu$ considered in this study, with the missing mass peaking around the ALP mass (M_a). However, such a contribution can be substantially reduced to 1%–7% of the total signal cross section (assuming comparable couplings) by making use of the same set of cuts prescribed in Sec. III B to reduce the SM background.

In specific UV completions of the low energy theory, all these effective couplings can be related to each other. However, their connection will be in general model dependent. For instance, one could have an additional vertex involving the Z boson, namely $\frac{C_{aZ\bar{\gamma}}}{\Lambda} a F_Z^{\mu\nu}\tilde{\bar{F}}_{\mu\nu}$, where $F_Z^{\mu\nu}$ is the Z field strength, related to the interactions in Eq. (1). In the following, we will take these couplings as independent parameters, assuming that the contribution from $C_{aZ\bar{\gamma}}$ is negligible with respect to the two photon's operators, and consider only the effects of the two dominant terms in Eq. (1).

Notice that the operators in Eq. (1) could induce a kinetic mixing term between the ordinary photon and the dark photon at one loop. However, in our study, we consider an unbroken $U(1)_D$ sector with a corresponding "massless" dark photon. This scenario is substantially different from the massive dark-photon one (including the case of ultralight but nonvanishing dark-photon masses). Indeed, as shown in [8], any mixing term between two $U(1)$ massless photons can be rotated away, by a redefinition of the corresponding fields. However, for a massless dark-photon scenario, after the rotation, the matter fields in the dark sector acquire an electromagnetic millicharged coupling. There are stringent laboratory constraints on millicharged particles [44–46], that mainly apply to masses below the GeV scale (see [44]), and relax if the millicharged sector gets quite heavy. In order to avoid potential laboratory and astrophysical constraints on millicharged particles, which might eventually constrain the couplings in Eq. (1), we assume the matter fields of dark sector to be quite heavy (i.e., above the 100 GeV scale) and unstable, so avoiding the severe constraints from millicharged dark matter [45].

For our collider analysis, we have considered ALP masses in the range $10\ {\rm GeV} \lesssim M_a \lesssim \sqrt{s}$, where $\sqrt{s}$ is the c.m. energy of e^+e^- collisions. Actually, the existing experimental limits related to ALP searches are mostly sensitive to a light ALP [in particular, lighter than $\mathcal{O}({\rm GeV})$], and come from, e.g., beam dump and light shining wall experiments, LSND and MiniBooNE experiments, lepton $g-2$ [5]. Given the ALP mass range we consider in the present analysis, most of the stringent bounds on the axion coupling $C_{a\gamma\gamma}/\Lambda$ in Eq. (1) carried out for very light ALPs can be neglected.

III. DARK-ALP PORTAL WITH HEAVY ALPS AT e^+e^- COLLIDERS

In order to probe both the ALP-photon-photon, $a\gamma\gamma$, and ALP-photon-dark-photon, $a\gamma\bar{\gamma}$, couplings, as defined in Eq. (1), we study the $e^+e^- \to \gamma\gamma\bar{\gamma}$ process at electron-positron colliders, where the dark photon $\bar{\gamma}$ behaves in the detector just like a neutrino, i.e., giving rise to massless missing momentum [47].

One of the main advantages of the diphoton+missing-energy channel over the conventional triphoton channel (associated to the process $e^+e^- \to a\gamma \to \gamma\gamma\gamma$) is the smaller SM background. As for illustration, at $\sqrt{s} \simeq M_Z$ the SM background in the *triphoton* channel is about 4 pb with nominal cuts on the photon energy ($E_\gamma > 2$ GeV) and rapidity ($|\eta| < 2.5$) along with the isolation between any photon pair ($\Delta R > 0.01$ where, $\Delta R = \sqrt{\Delta\eta^2 + \Delta\phi^2}$), whereas that in the diphoton+missing-energy channel coming from $\gamma\gamma\nu\bar{\nu}$ production is about 0.1 pb. As we will see from our results, the diphoton+missing-energy channel gives more than an order-of-magnitude improvement in the coupling constraints over the triphoton channel, when the corresponding couplings are comparable (e.g., $C_{a\gamma\gamma} \simeq C_{a\gamma\bar{\gamma}} \simeq 1$). However, here we focus on the diphoton+missing-energy channel not merely as an improvement over the triphoton one, but mainly as a further independent search channel for ALPs in presence of both $C_{a\gamma\gamma}$ and $C_{a\gamma\bar{\gamma}}$ nonvanishing couplings. In particular, we will see that in the region of the $(C_{a\gamma\gamma}, C_{a\gamma\bar{\gamma}})$ plane beyond the reach of the

[2]The factor 2 in the second term has been introduced to take into account the effect of the Wick contractions in the first term arising from the matrix element with two external photon states.

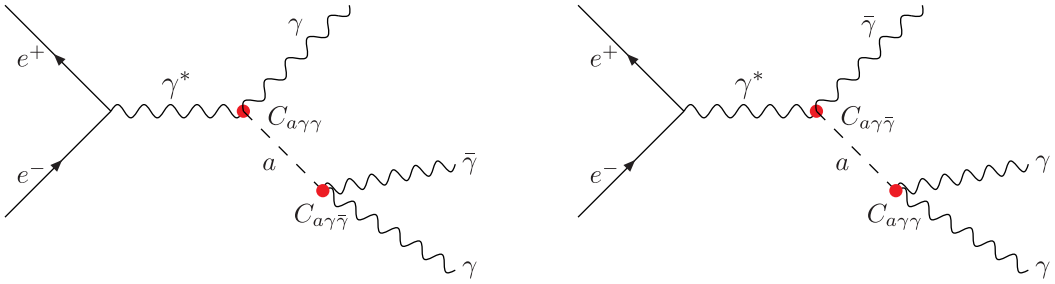

FIG. 1. Feynman diagrams for the signal subprocesses $e^+e^- \to \gamma a \to \gamma\gamma\bar{\gamma}$ and $e^+e^- \to \bar{\gamma}a \to \gamma\gamma\bar{\gamma}$.

triphoton channel (e.g., the region where $C_{a\gamma\gamma} \ll C_{a\gamma\bar{\gamma}}$), the diphoton+missing-energy channel may become a more effective and independent probe of ALPs.

As collision c.m. energy, we consider the energies foreseen by the FCC-ee present staging, that is $\sqrt{s} \simeq [M_Z, 160\ \text{GeV}, 240\ \text{GeV}]$, with integrated luminosity $\text{L} \simeq [150, 10, 5] ab^{-1}$, respectively [43] (leaving aside here possible higher energy runs at $\sqrt{s} \simeq 365$ GeV). The corresponding results for the ILC and CEPC cases, and some extrapolation to the CLIC energies, can be anyway obtained in a quite straightforward way from the present discussion.

The $e^+e^- \to \gamma\gamma\bar{\gamma}$ process arises from the couplings in Eq. (1) via the Feynman diagrams detailed in Fig. 1. The two diagrams interfere in a constructive way. Assuming $C_{a\gamma\gamma} = C_{a\gamma\bar{\gamma}} = 1$, the contribution due to interference varies from 4% to about 17% of the total cross section within the ALP mass range considered in these analyses. The dominant contributions come from the incoherent sum of the individual subprocesses. The impact of interference effects can of course change as one moves away from the $C_{a\gamma\gamma} = C_{a\gamma\bar{\gamma}} = 1$ assumption (a similar behavior affects the ALP total width corresponding to the decays $a \to \gamma\bar{\gamma}, \gamma\gamma$).

In the $e^+e^- \to \gamma\gamma\bar{\gamma}$ process, the ALP is produced on shell, and it further undergoes a two-body decay to $\gamma\gamma$ or $\gamma\bar{\gamma}$. This helps a lot in the characterization of the signal versus the SM background, which is mainly arising from the $e^+e^- \to \gamma\gamma\bar{\nu}\nu$ process, for an invisible dark photon. Indeed, one can treat the signal events as a $2 \to 2 \to 3$ process (modulo interference effects) and the momenta of the final state particles are correspondingly constrained, with different constraints for different subprocesses. On the other hand, the background $e^+e^- \to \gamma\gamma\bar{\nu}\nu$ is characterized by $2 \to 4$ and $2 \to 3 \to 4$ subprocesses, and the corresponding phase-space behavior is in general significantly different from the signal one. The presence of the missing momentum associated to a single invisible massless dark photon in the final state will provide a crucial additional handle to separate the signal from the SM background.

In the following, we use the MadGraph5 event generator [48] to simulate both the signal and the background events. We have implemented the effective ALP vertices using the FeynRules packages (v2.0) [49]. The output of the FeynRules (UFO model files) is then interfaced with MadGraph5 (v2.6.3.2).

A. LEP analysis

The effective $a\gamma\bar{\gamma}$ interactions between the ALP, photon, and dark photon can already be tested and constrained using the existing LEP data [50]. The L3 Collaboration searched for single or multiphoton events with missing energy arising from $e^+e^- \to \bar{\nu}\nu\gamma(\gamma)$, in the c.m. energy range $\sqrt{s} = (189 - 208)$ GeV, with a total integrated luminosity of 619 pb^{-1}. In Table I, we show the number of predicted signal events in our model, and the expected SM background events, along with the observed data in the multiphoton+missing-energy channel, after applying the set of cuts described in [50].

We have also estimated the corresponding 2σ exclusion limits on the model parameters (i.e., $C_{a\gamma\gamma}$ and $C_{a\gamma\bar{\gamma}}$, at fixed M_a and Λ) coming from the LEP analysis and presented them in the following sections. Note that the LEP analysis of the multiphoton+missing-energy channel has not been optimized for the $e^+e^- \to \gamma\gamma\bar{\gamma}$ process. In the next subsection, we will discuss the relevant optimization strategy in the context of future e^+e^- colliders.

B. Future e^+e^- colliders

In this section, we discuss the prospect of the $e^+e^- \to \gamma\gamma\bar{\gamma}$ in the context of future e^+e^- colliders. We start by discussing the signal cross section and the event selection criteria taking into account various kinematical

TABLE I. Number of predicted signal events in our model (assuming $C_{a\gamma\gamma} = C_{a\gamma\bar{\gamma}} = 1$ and $\Lambda = 1$ TeV), in the multiphoton +missing-energy final state, with an integrated luminosity of 619 pb^{-1}, in the range $\sqrt{s} = (189 - 208)$ GeV, after applying the selection described in [50]. The expected SM events and the observed ones are also presented in the last two rows, respectively, showing no excess in the data.

M_a (GeV)	$N_{\text{events}}(n\gamma + \not{E})_{\text{LEP}}$
10	304
50	810
80	583
150	77.8
190	1.92
Expected (SM)	115
Observed	101

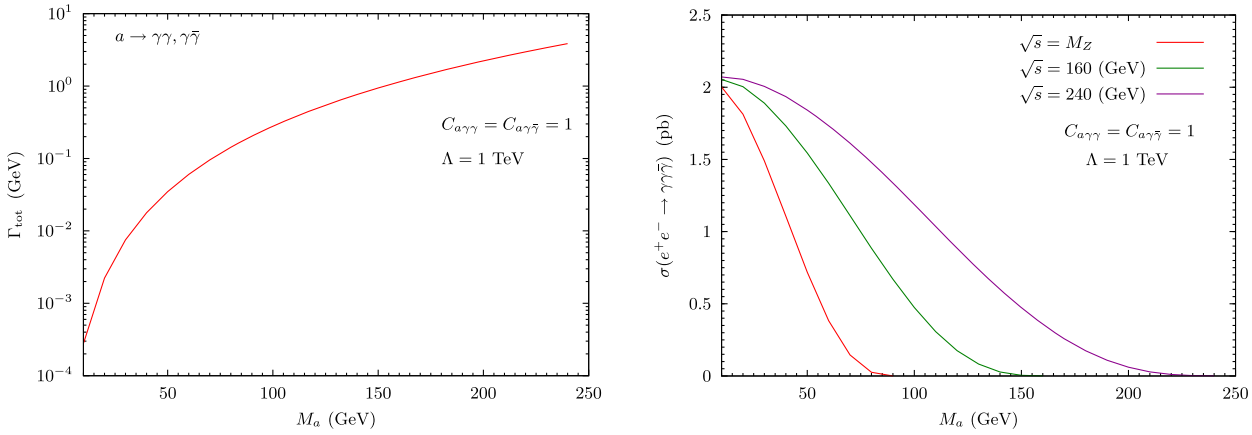

FIG. 2. The left figure shows the variation of the ALP total decay width ($\Gamma_{\rm tot}$), as a function of the ALP mass M_a. The right figure shows the total cross section $\sigma(e^+e^- \to \gamma\gamma\bar{\gamma})$ at different c.m. energies versus the ALP mass in the range 10 GeV $\lesssim M_a \lesssim \sqrt{s}$. We assume $C_{a\gamma\gamma} = C_{a\gamma\bar{\gamma}} = 1$ and $\Lambda = 1$ TeV. The cross section presented is the leading-order one, not including the contribution from the process with extra photons from initial-state radiation.

distributions. First, we plot in Fig. 2 the ALP total decay width (left) and the total $e^+e^- \to \gamma\gamma\bar{\gamma}$ cross section (right) versus the ALP mass, assuming $C_{a\gamma\gamma} = C_{a\gamma\bar{\gamma}} = 1$ and $\Lambda = 1$ TeV. The left plot shows how, even for ALP masses as low as 10 GeV, the ALP is not stable on the detector length scale down to couplings of the order $C_{a\gamma\gamma}, C_{a\gamma\bar{\gamma}} \sim 10^{-4}$, with $\Lambda \sim 1$ TeV, for which the decay length is of the order of 0.1 mm. For narrower ALP widths, a displaced-vertices strategy might be in order.

In order to account for initial-state radiation effects, we have also added the radiative contribution of the $e^+e^- \to \gamma\gamma\gamma\bar{\gamma}$ and $e^+e^- \to \gamma\gamma\bar{\nu}\nu$ processes to the signal and background, respectively.

The effect of finite detector resolution on the energy of each photon has been incorporated with a Gaussian smearing function parametrized as in a typical ILC detector,

$$\frac{\Delta E}{E} = \frac{16.6\%}{\sqrt{E/\mathrm{GeV}}} \oplus 1.1\%. \tag{2}$$

In order to reconstruct signal events as events containing at least two isolated photons with some missing energy, we impose the following set of basic cuts on the final-state observables (in the following, we call C1 this set of basic cuts for the diphoton+missing-energy events):

(i) Minimum energy for each photon, $E_\gamma > 2$. GeV.
(ii) Maximum rapidity for each photon, $|\eta_\gamma| < 2.5$.
(iii) Angular separation between any pair of photons greater than 15°.
(iv) Minimum missing transverse energy, $\not{E}_T > 5$. GeV.

In Fig. 3, we plot the normalized distributions for the missing energy $\not{E}$ associated to the dark photon (or, in the background case, to the $\bar{\nu}\nu$ system), and for the hardest-photon energy E_{γ_1}, for signal and background, at a c.m.

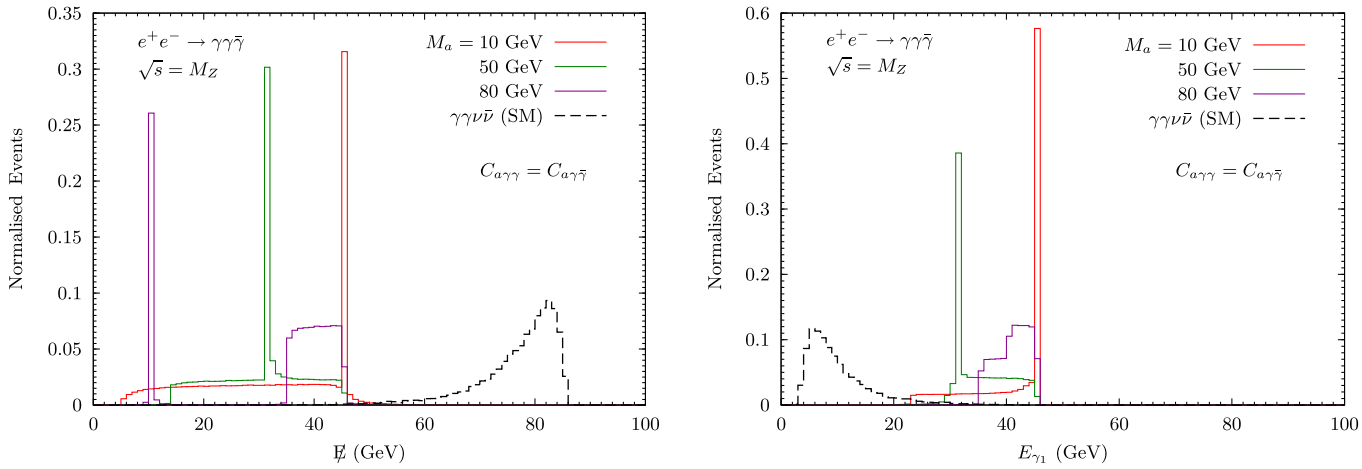

FIG. 3. Missing-energy ($\not{E}$) and hardest-photon energy (E_{γ_1}) distributions in the $e^+e^- \to \gamma\gamma + \not{E}$ final state at $\sqrt{s} \simeq M_Z$, for a few ALP-mass benchmarks and the SM background ($\gamma\gamma\nu\bar{\nu}$). The basic cuts applied are the C1 set as defined in the text.

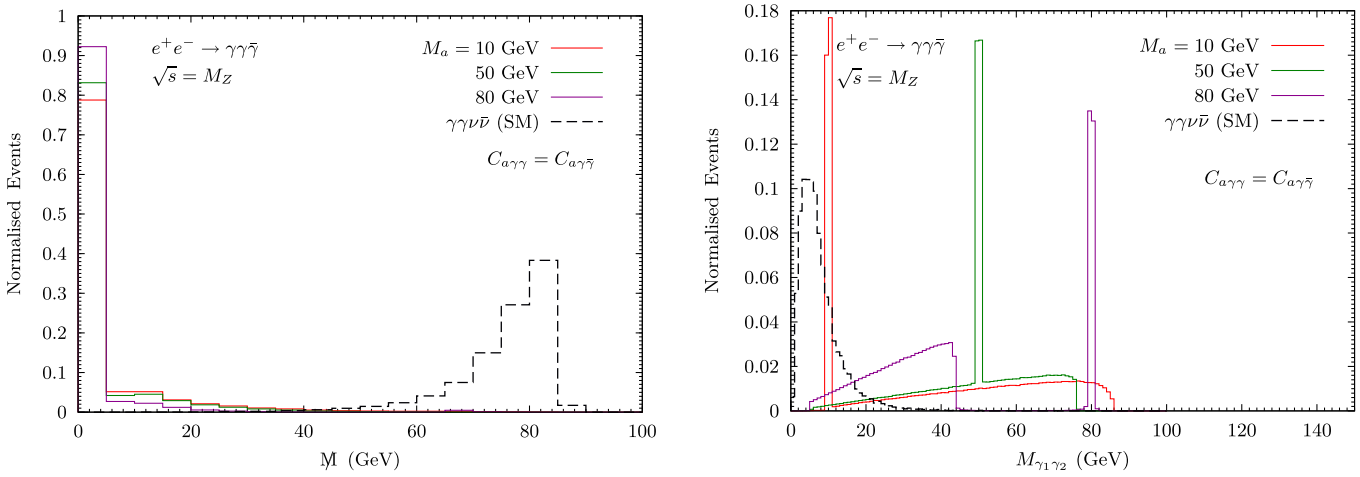

FIG. 4. Missing-mass ($\not{M}$) and diphoton invariant mass ($M_{\gamma\gamma}$) distributions in the $e^+e^- \to \gamma\gamma + \not{E}$ final state at $\sqrt{s} \simeq M_Z$, for a few ALP-mass benchmarks and the SM background ($\gamma\gamma\nu\bar{\nu}$). The basic cuts applied are the C1 set as defined in the text.

energy $\sqrt{s} \simeq M_Z$. Figure 4 shows the missing-mass $\not{M}$ distribution associated to the invisible system (with $\not{M}$ defined below), and the diphoton-system invariant mass distribution, for signal and background. The same is shown in Figs. 5–8 at different c.m. energies, namely, $\sqrt{s} = 160$ and 240 GeV. All these distributions have been obtained after applying the set of basic cuts C1, mentioned above.

In general, the shape of the $\not{E}$ distributions for the signal contains a peak superimposed on a box distribution. This corresponds to the different kinematics associated the two subprocesses where either a $\gamma\bar{\gamma}$ or a $\gamma\gamma$ system is resonating at the ALP mass (see Fig. 1). In one case, the ALP is produced in association with a photon, giving rise to the box distribution for the dark photon which arises from the ALP decay. In the second case, the ALP is produced in association with the dark photon, which is essentially monochromatic. The peak position corresponding to the monochromatic component in the $\not{E}$ distribution is given by

$$\not{E}_{\text{peak}} \simeq \frac{\sqrt{s}}{2}\left(1 - \frac{M_a^2}{s}\right), \tag{3}$$

while the minima and maxima of the box distributions are given by

$$\not{E}_{\text{min}} \simeq \frac{1}{2}\frac{M_a^2}{\sqrt{s}}, \qquad \not{E}_{\text{max}} \simeq \frac{\sqrt{s}}{2}. \tag{4}$$

When $M_a \approx \sqrt{s}$, the distribution splits up into two separate kinematical regions for a given M_a, because $\not{E}_{\text{peak}} \ll \not{E}_{\text{min}} \approx \not{E}_{\text{max}}$. On the other hand, for $0 \lesssim M_a \lesssim \sqrt{s/2}$, the peak lies between the $\not{E}_{\text{min}}$ and $\not{E}_{\text{max}}$ ($\not{E}_{\text{min}} < \not{E}_{\text{peak}} < \not{E}_{\text{max}}$). This is clearly shown in Figs. 3, 5, and 7.

In addition to the $\not{E}$ variable, we have introduced the invariant mass of the invisible system [47]. The invariant

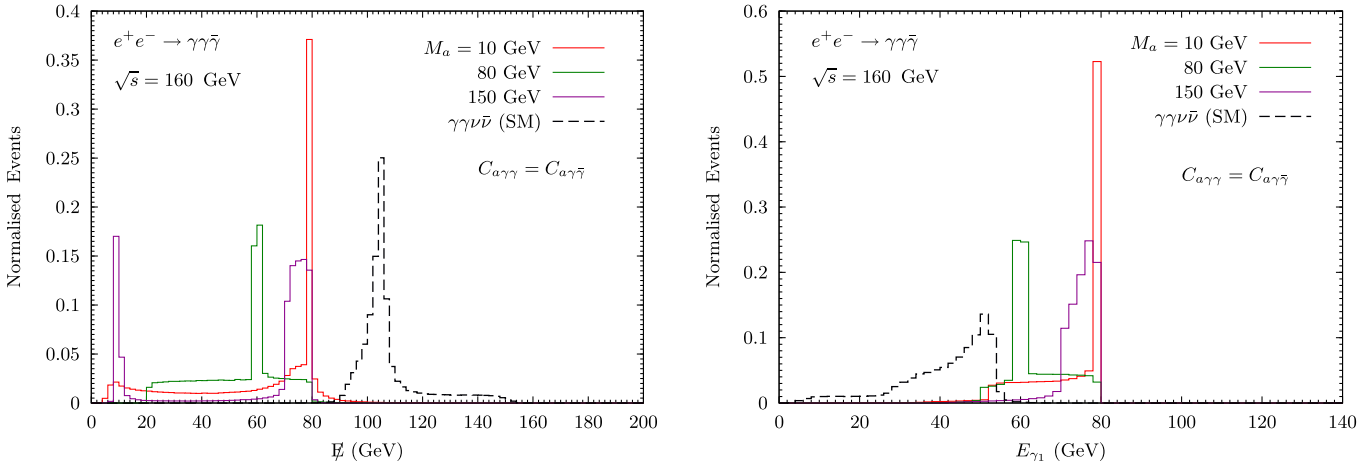

FIG. 5. Missing-energy ($\not{E}$) and hardest-photon energy (E_{γ_1}) distributions in the $e^+e^- \to \gamma\gamma + \not{E}$ final state at $\sqrt{s} = 160$ GeV, for a few ALP-mass benchmarks and the SM background ($\gamma\gamma\nu\bar{\nu}$). The basic cuts applied are the C1 set as defined in the text.

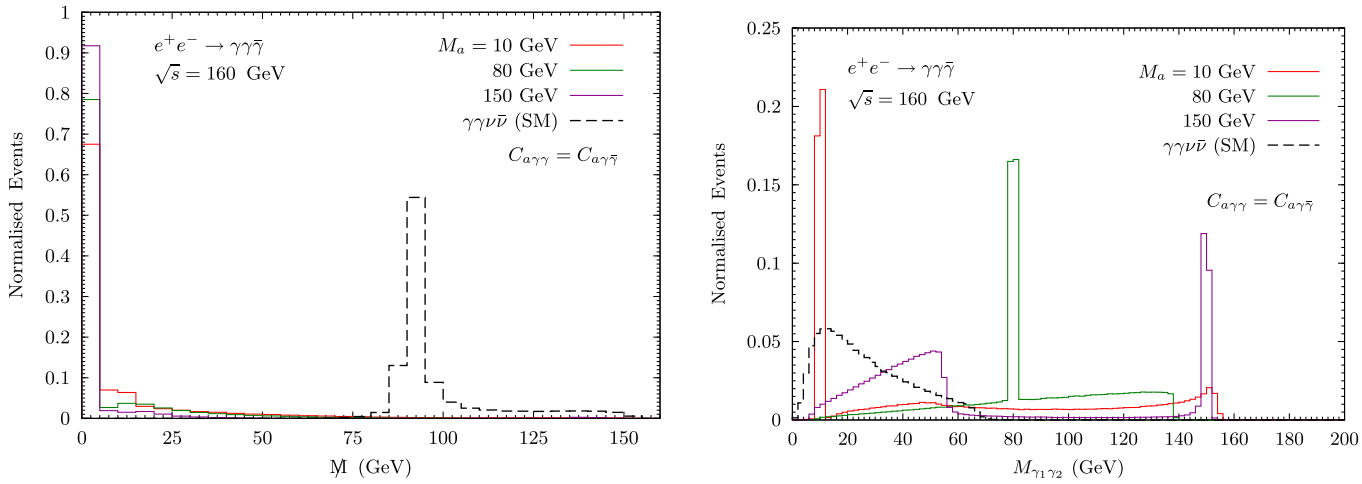

FIG. 6. Missing-mass ($\not{M}$) and diphoton invariant mass ($M_{\gamma\gamma}$) distributions in the $e^+e^- \to \gamma\gamma + \not{E}$ final state at $\sqrt{s} = 160$ GeV, for a few ALP-mass benchmarks and the SM background ($\gamma\gamma\nu\bar{\nu}$). The basic cuts applied are the C1 set as defined in the text.

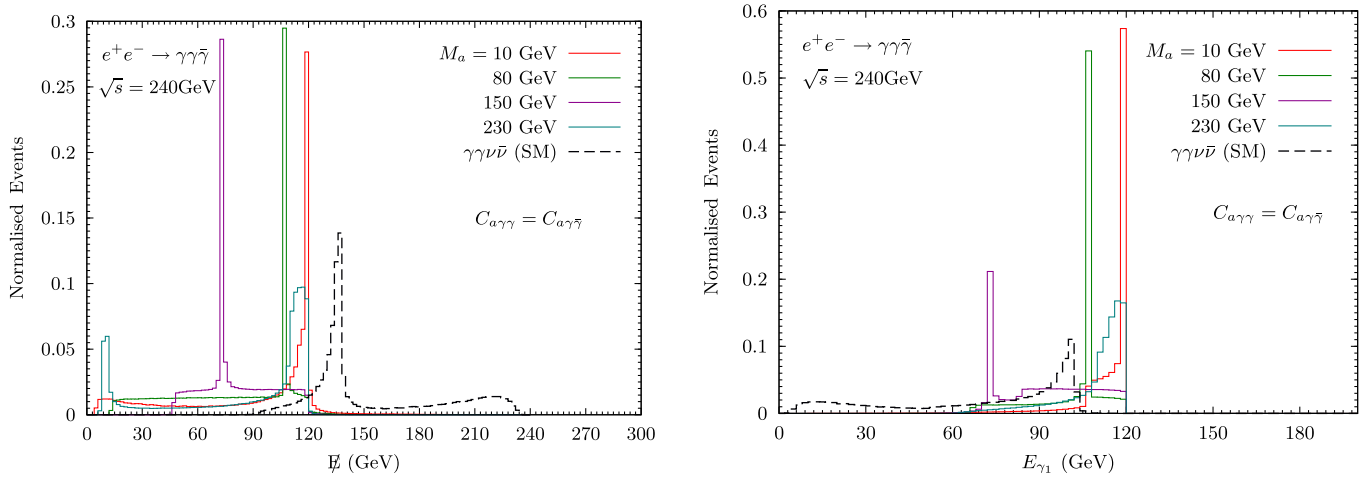

FIG. 7. Missing-energy ($\not{E}$) and hardest-photon energy (E_{γ_1}) distributions in the $e^+e^- \to \gamma\gamma + \not{E}$ final state at $\sqrt{s} = 240$ GeV, for a few ALP-mass benchmarks and the SM background ($\gamma\gamma\nu\bar{\nu}$). The basic cuts applied are the C1 set as defined in the text.

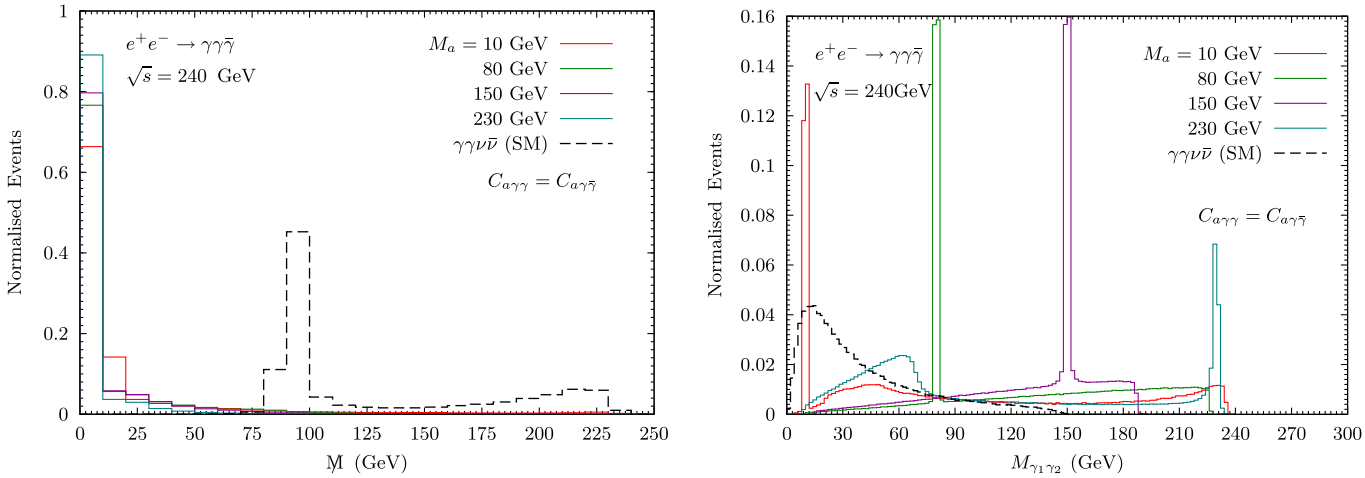

FIG. 8. Missing-mass ($\not{M}$) and diphoton invariant mass ($M_{\gamma\gamma}$) distributions in the $e^+e^- \to \gamma\gamma + \not{E}$ final state at $\sqrt{s} = 240$ GeV, for a few ALP-mass benchmarks and the SM background ($\gamma\gamma\nu\bar{\nu}$). The basic cuts applied are the C1 set as defined in the text.

mass of the invisible system (or missing mass) $\not{M}$ is defined as

$$\not{M} = \sqrt{\not{E}^2 - \vec{\not{P}}^2} \tag{5}$$

and turns out to be a crucial variable to separate the signal from the SM background.

Indeed, the signal invisible momentum is carried by the dark photon which is massless in our scenario. Therefore, the missing mass is expected to peak near zero. On the contrary, the background invisible momentum is carried by the $\bar{\nu}\nu$ system for which the mass distribution is expected to be dominant at quite large values.

We extensively make use of the $\not{E}$ and $\not{M}$ kinematical variables to separate the signal from the SM background. To this end, we set an upper limit on the missing energy and the missing mass associated with the accepted events. These two variables are quite independent, unless one fixes the invariant mass of the diphoton system $M_{\gamma\gamma}$, on which we actually do not put any constraint.

On the basis of the above distributions, we will impose a cut $\not{M} < 10$ GeV, and a cut $\not{E} < \sqrt{s}/2$, in order to optimize the signal significance, for the following choice of $\sqrt{s}$ and M_a parameters:

(i) $\sqrt{s} \simeq M_Z$, 10 GeV $\lesssim M_a \lesssim$ 80 GeV.
(ii) $\sqrt{s} = 160$ GeV, 10 GeV $\lesssim M_a \lesssim$ 150 GeV.
(iii) $\sqrt{s} = 240$ GeV, 10 GeV $\lesssim M_a \lesssim$ 230 GeV.

We also compare our diphoton+missing-energy channel's performance with the existing searches for ALPs in the triphoton channel by making use of the analysis detailed in [26]. Since the selection cuts described in this reference have already been optimized for different ALP masses and e^+e^- collision energies, we adopt their analysis to give a projection in the triphoton channel at future e^+e^- colliders.

IV. RESULTS AND DISCUSSION

We now present the results of our analyses. The final choice of the event selection criteria is a natural consequence of the kinematic distributions discussed in the previous section. The combination of the missing-energy $\not{E}$ and missing-mass $\not{M}$ cuts reduces the SM background substantially. For $\sqrt{s} \simeq M_Z$ and 160 GeV, the optimized choice of cuts is independent of the ALP masses. This is because both the missing-energy and the missing-mass distributions have very small or almost negligible overlap with background events. On the other hand, on the basis of $\not{E}$ distributions, a mild M_a dependence is expected at $\sqrt{s} = 240$ GeV. However, we could obtain a significance very close to one corresponding to the M_a dependent optimized cuts, by adopting the same (rescaled) cut choice as used at lower $\sqrt{s}$.

In Tables II–IV, we present the numerical results of our analysis for a few representative M_a benchmarks in order to illustrate the effects of the cut flow on the signal and the background events discussed earlier, at various e^+e^- collision energies. The signal events reported correspond to $C_{a\gamma\gamma} = C_{a\gamma\bar{\gamma}} = 1$ and $\Lambda = 1$ TeV and can be easily rescaled for different couplings and energy scale. We name σ_{cut}, the residual cross sections after applying the complete cut flow to the process phase space.

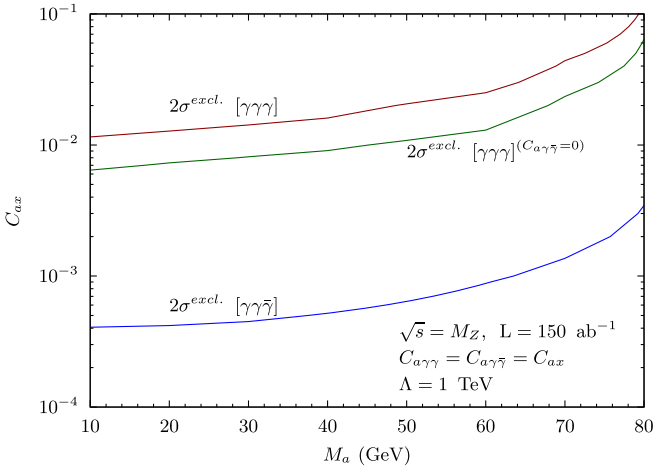

FIG. 9. The 2σ exclusion limit in the (C_{ax}, M_a) plane coming from the triphoton ($[\gamma\gamma\gamma]$) and diphoton+missing-energy ($[\gamma\gamma\bar{\gamma}]$) channels at $\sqrt{s} \simeq M_Z$, for an integrated luminosity of 150 ab^{-1}, assuming $C_{a\gamma\gamma} = C_{a\gamma\bar{\gamma}} = C_{ax}$ and $\Lambda = 1$ TeV. The curve in green line represents 2σ exclusion limit obtained in the triphoton channel by setting $C_{a\gamma\bar{\gamma}} = 0$.

In Figures 9–11, we present and compare the exclusion limits coming from the triphoton ($[\gamma\gamma\gamma]$) and diphoton +missing-energy ($[\gamma\gamma\bar{\gamma}]$) channels in the (C_{ax}, M_a) plane, assuming $C_{a\gamma\gamma} = C_{a\gamma\bar{\gamma}} = C_{ax}$, for various c.m. energies and corresponding expected integrated luminosities.

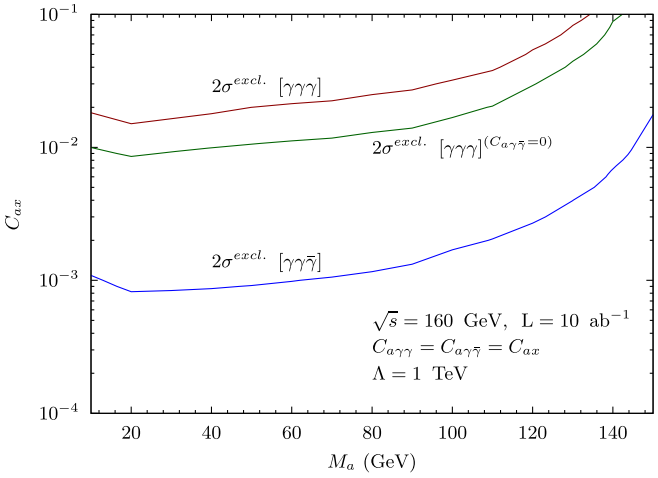

FIG. 10. The 2σ exclusion limit in the (C_{ax}, M_a) plane coming from the triphoton ($[\gamma\gamma\gamma]$) and diphoton + missing-energy ($[\gamma\gamma\bar{\gamma}]$) channels at $\sqrt{s} = 160$ GeV, for an integrated luminosity of 10ab^{-1}, assuming $C_{a\gamma\gamma} = C_{a\gamma\bar{\gamma}} = C_{ax}$, and $\Lambda = 1$ TeV. The curve in green line represents 2σ exclusion limit obtained in the triphoton channel by setting $C_{a\gamma\bar{\gamma}} = 0$.

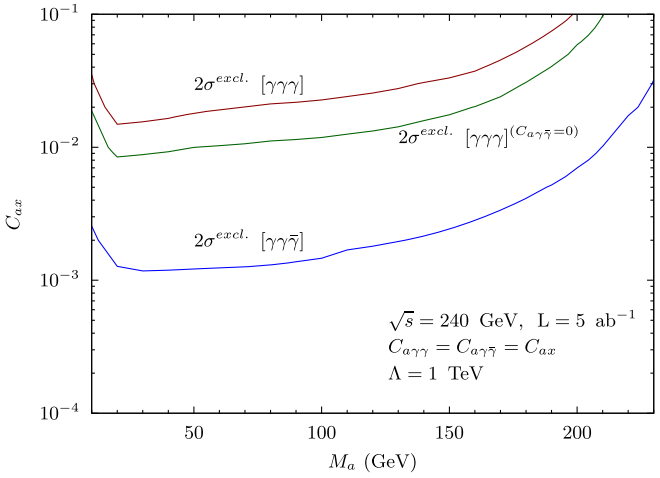

FIG. 11. The 2σ exclusion limit in the (C_{ax}, M_a) plane coming from the triphoton ($[\gamma\gamma\gamma]$) and diphoton + missing-energy ($[\gamma\gamma\bar{\gamma}]$) channels at $\sqrt{s} = 240$ GeV, for an integrated luminosity of 5 ab^{-1}, assuming $C_{a\gamma\gamma} = C_{a\gamma\bar{\gamma}} = C_{ax}$, and $\Lambda = 1$ TeV. The curve in green line represents 2σ exclusion limit obtained in the triphoton channel by setting $C_{a\gamma\bar{\gamma}} = 0$.

The corresponding exclusion limits for a vanishing $C_{a\gamma\bar{\gamma}}$ coupling in the triphoton ($[\gamma\gamma\gamma]^{(C_{a\gamma\bar{\gamma}}=0)}$) channel have also been included in the same plots (by curves in green line).

The 2σ limit has been obtained by assuming for the signal significance the following definition:

$$\tilde{\sigma} = \sqrt{2[(S+B)\ln(1+S/B) - S]}, \tag{6}$$

where S and B are the numbers of observed signal and background events, respectively, corresponding to the residual signal and background cross sections $\sigma_{\rm cut}$ in Tables II–IV. One can see that the diphoton+missing-energy channel is more sensitive compared to the triphoton channel for comparable couplings. The former channel also provides stronger bounds on $C_{a\gamma\gamma}$ even for tiny but significant $C_{a\gamma\bar{\gamma}}$ (e.g., $C_{a\gamma\bar{\gamma}} \sim 10^{-3}$) compared to the case where $C_{a\gamma\bar{\gamma}} = 0$.

From Figures 9–11, one can also see that the 2σ reach for $M_a \sim 10$ GeV is less sensitive compared to the one for $M_a \sim 20$ GeV, at $\sqrt{s} = 160$ and 240 GeV, despite the large production cross section in this mass region. The decrease in sensitivity at low M_a is due to the effect of the photon isolation requirement when the two photons coming from the ALP decay are mostly collimated. This effectively reduces the cut efficiency. On the other hand, the 2σ limit on the couplings becomes less sensitive at larger M_a values, because of the corresponding lower production cross section. It is very much evident from these plots that for masses $M_a \lesssim 60$ GeV, the best exclusion limit is achieved at $\sqrt{s} \simeq M_Z$. This is because of the very high expected integrated luminosity of about 150 ab^{-1} at this energy, despite the comparatively lower signal cross sections. For 60 GeV$\lesssim M_a \lesssim$ 90 GeV, a slightly better sensitivity is obtained at $\sqrt{s} = 160$ GeV, where a factor-2 enhancement in luminosity with respect to $\sqrt{s} = 240$ GeV more than compensates the enhancement in the production cross section at higher collision energy.

In Figs. 12 and 13, we also plot the 2σ exclusion contours in the $(C_{a\gamma\gamma}, C_{a\gamma\bar{\gamma}})$ plane for fixed M_a. The red, purple, and green lines represent the bounds obtained from the analysis discussed in Sec. III B.

The black dashed curve represents the bound coming from the LEP analysis (as described in Sec. III A), by

TABLE II. Cross sections (before and after cuts) and event counts out of 10^6 simulated events, for the signal and the SM $\gamma\gamma\nu\bar{\nu}$ background at $\sqrt{s} \simeq M_Z$ (versus M_a), applying the C1 set of basic cuts as described in the text, followed by further sequential cut optimization. We assume $C_{a\gamma\gamma} = C_{a\gamma\bar{\gamma}} = 1$ and $\Lambda = 1$ TeV.

$\sqrt{s} \simeq M_Z$		$N_{\rm events}$			
M_a (GeV)	$\sigma_{\rm tot}$ (fb)	Basic cuts	$\not{E} < 46$ GeV	$\not{M} < 10$ GeV	$\sigma_{\rm cut}$ (fb)
10	2002	839514	813996	704647	1410
50	719	935228	929024	813901	585
80	25.9	877285	874469	833578	21.7
$\gamma\gamma\nu\bar{\nu}$	2544	12884	44	1	0.0025

TABLE III. Cross sections (before and after cuts) and event counts out of 10^6 simulated events, for the signal and the SM $\gamma\gamma\nu\bar{\nu}$ background at $\sqrt{s} = 160$ GeV (versus M_a), applying the C1 set of basic cuts as described in the text, followed by further sequential cut optimization. We assume $C_{a\gamma\gamma} = C_{a\gamma\bar{\gamma}} = 1$ and $\Lambda = 1$ TeV.

$\sqrt{s} = 160$ GeV		$N_{\rm events}$			
M_a (GeV)	$\sigma_{\rm tot}$ (fb)	Basic cuts	$\not{E} < 80$ GeV	$\not{M} < 10$ GeV	$\sigma_{\rm cut}$ (fb)
10	2054	511509	476414	381606	784
80	885	950028	942370	773597	685
150	4.62	882485	878570	818390	3.78
$\gamma\gamma\nu\bar{\nu}$	3089	186189	133	1	0.0031

TABLE IV. Cross sections (before and after cuts) and event counts out of 10^6 simulated events, for the signal and the SM $\gamma\gamma\nu\bar{\nu}$ background at $\sqrt{s} = 240$ GeV (versus M_a), applying the C1 set of basic cuts as described in the text, followed by further sequential cut optimization. We assume $C_{a\gamma\gamma} = C_{a\gamma\bar{\gamma}} = 1$ and $\Lambda = 1$ TeV.

$\sqrt{s} = 240$ GeV		$N_{\rm events}$			
M_a (GeV)	$\sigma_{\rm tot}$ (fb)	Basic cuts	$\not{E} < 120$ GeV	$\not{M} < 10$ GeV	$\sigma_{\rm cut}$ (fb)
10	2071	245025	229988	163157	338
80	1478	954942	941647	728484	1077
150	473	947603	941097	753879	356
230	2.92	912354	907124	798522	2.33
$\gamma\gamma\nu\bar{\nu}$	1615	175959	16729	5	0.0081

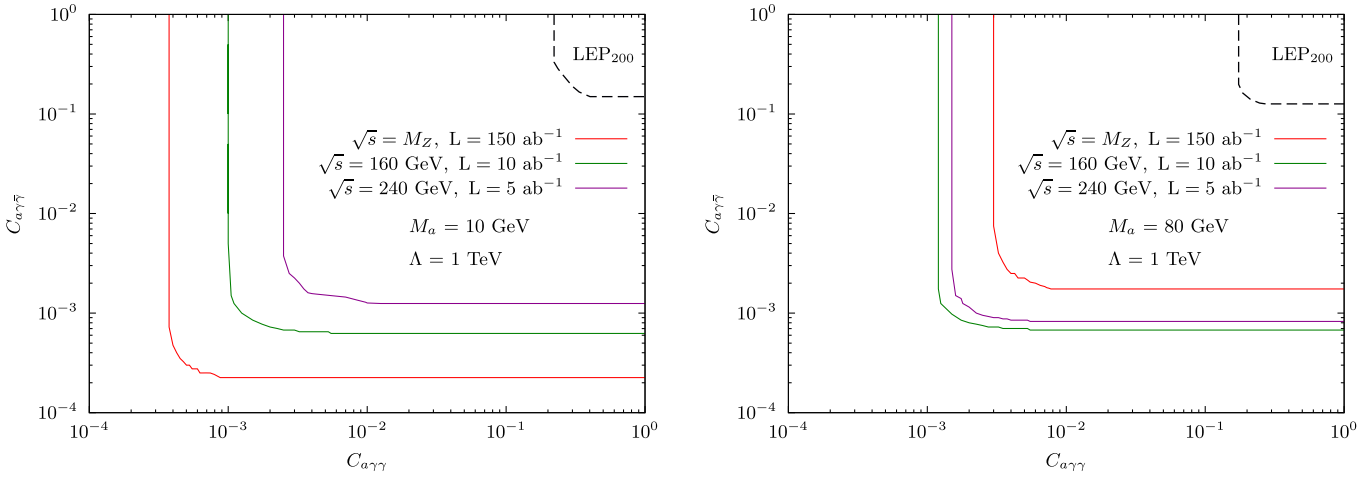

FIG. 12. The 2σ exclusion limits in the $(C_{a\gamma\gamma}, C_{a\gamma\bar{\gamma}})$ plane for fixed M_a (left $M_a = 10$ GeV, right $M_a = 80$ GeV). The colored lines (red, green, and purple) depict the bound coming from the analysis at $\sqrt{s} \simeq M_Z$, 160 GeV, and 240 GeV, for an integrated luminosity of 150 ab^{-1}, 10 ab^{-1}, and 5 ab^{-1}, respectively, and the black dashed line represents the bound coming from the LEP analysis as described in the text. We have assumed $\Lambda = 1$ TeV.

assuming a null result. In these plots, we dubbed LEP$_{200}$ the LEP searches in the range $\sqrt{s} = (189 - 208)$ GeV, with a total integrated luminosity of 619 pb^{-1} [50]. From the two-dimensional plots, it is also clear that the future collider experiments will be much more sensitive and have much better reach in the $(C_{a\gamma\gamma}, C_{a\gamma\bar{\gamma}})$ plane, thanks to both a higher luminosity and to the optimized selection strategy. The significance definition in Eq. (6) is used everywhere to make this comparison.

One can notice from the plots in Figs. 12 and 13, that when one of the couplings is much lower than the other, the sensitivity to the smaller coupling is independent of the latter. This feature arises from the scaling of the cross section with the couplings, when ignoring interference effects. Indeed, the cross section for the $e^+e^- \to \gamma\gamma\bar{\gamma}$ process scales as $\sigma(e^+e^- \to \gamma\gamma\bar{\gamma}) \approx C^2_{a\gamma\gamma}[\sigma_1 + \frac{\Gamma_1}{\Gamma_2}\sigma_2]$ for $C_{a\gamma\gamma} \ll C_{a\gamma\bar{\gamma}}$, while for $C_{a\gamma\bar{\gamma}} \ll C_{a\gamma\gamma}$ the scaling is given by $\sigma(e^+e^- \to \gamma\gamma\bar{\gamma}) \approx C^2_{a\gamma\bar{\gamma}}[\frac{\Gamma_2}{\Gamma_1}\sigma_1 + \sigma_2]$ [where the factors $\sigma_1 = \sigma(e^+e^- \to \gamma a)$, $\sigma_2 = \sigma(e^+e^- \to \bar{\gamma} a)$, $\Gamma_1 = \Gamma(a \to \gamma\gamma)$, and $\Gamma_2 = \Gamma(a \to \gamma\bar{\gamma})$ are all evaluated at $C_{a\gamma\gamma} = C_{a\gamma\bar{\gamma}} = 1$ and $\Lambda = 1$ TeV]. Therefore, the total cross section in either of these limits roughly scales with the smallest of the two couplings squared and becomes independent of the other.

Furthermore, the sensitivity of the exclusion limit in the $(C_{a\gamma\gamma}, C_{a\gamma\bar{\gamma}})$ plane for fixed M_a is not symmetric in the two couplings. The sensitivity reach for $C_{a\gamma\bar{\gamma}}$ is indeed slightly better than that for $C_{a\gamma\gamma}$. This is because, the partial widths

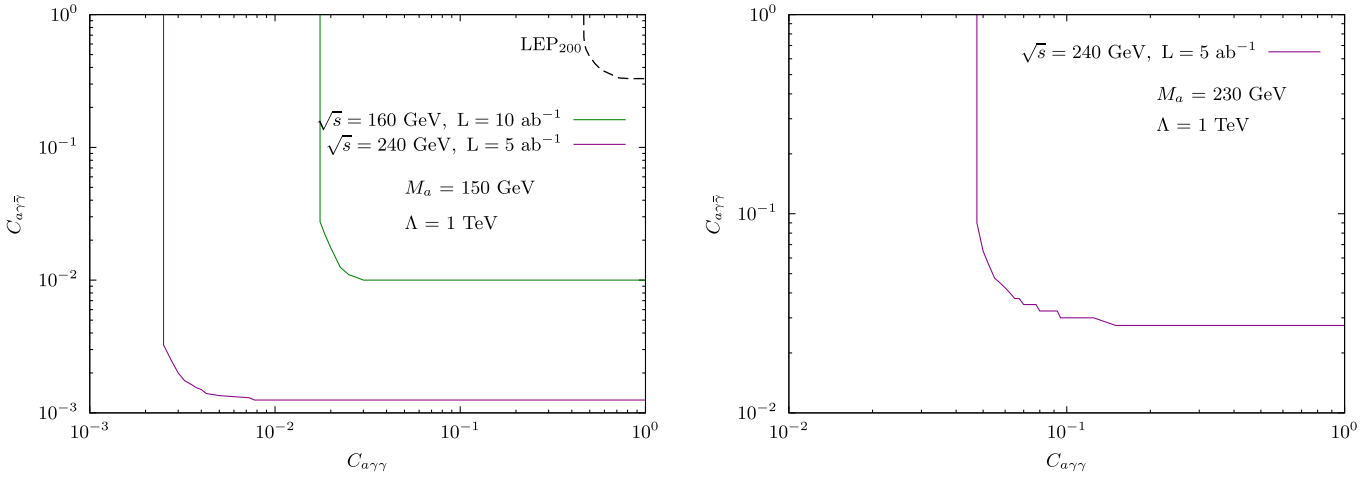

FIG. 13. The 2σ exclusion limits in the $(C_{a\gamma\gamma}, C_{a\gamma\bar{\gamma}})$ plane for fixed M_a and given $\sqrt{s}$ (left: $M_a = 150$ GeV at $\sqrt{s} = 160$ GeV and 240 GeV (green and purple lines), right: $M_a = 230$ GeV at $\sqrt{s} = 240$ GeV (purple line)), for integrated luminosities as shown. The black dashed line in the left figure represents the bound coming from the LEP analysis as described in the text, for $M_a = 150$ GeV. We have assumed $\Lambda = 1$ TeV.

Γ_2 and Γ_1 enter in the expression for the cross sections describing the scaling (just defined) in inverted ratios, and $\frac{\Gamma_2}{\Gamma_1} > 1$.

Figures 12 and 13 indeed show that, when there is a clear hierarchy in the $a\gamma\gamma$ and $a\gamma\bar{\gamma}$ couplings, the 2σ exclusion dependence is restricted to just the smallest coupling. However, in case a $e^+e^- \to \gamma\gamma\bar{\gamma}$ signal is detected, our analysis would not be able to distinguish the corresponding hierarchical ordering of the two couplings.

V. SUMMARY AND CONCLUSIONS

We have considered an axionlike particle with mass in the range (10–230) GeV, coupled to a photon and a massless dark photon through higher-dimensional effective operators. Such operators may occur naturally in a theory which includes light pseudoscalar and dark-photon particles and can be generated at the loop level by heavy messenger particles charged under both $U(1)_{\rm em}$ and $U(1)_D$. We have investigated the future collider prospects for a scenario including these effective operators. In particular, we have thoroughly studied and lay down the strategy to probe a dark-ALP portal as defined in Eq. (1), at future e^+e^- colliders. The conventional search for *three-photon* final states (which does not include the $a\gamma\bar{\gamma}$ coupling) is replaced by the $2\gamma + \not{E}$ signature arising from the $e^+e^- \to \gamma\gamma\bar{\gamma}$ process, with the missing momentum arising from the dark photon in the collision final state well characterized by a vanishing missing mass. We assumed a prompt ALP decay on a typical-detector length scale. The main SM background coming from the $e^+e^- \to \gamma\gamma\nu\bar{\nu}$ channel can then be controlled by proper cut flows on the most sensitive kinematic variables, namely the missing energy $\not{E}$ and missing mass $\not{M}$. Relevant kinematical distributions and consequent selection strategies for the $e^+e^- \to \gamma\gamma\bar{\gamma}$ process have been analyzed. The missing-mass variable associated to the dark photon turns out to be particularly efficient for the S/B optimization. Projections at future e^+e^- colliders for the corresponding constraints on the $a\gamma\gamma$ and $a\gamma\bar{\gamma}$ couplings have been discussed. For ALP masses not too close to the production threshold, the FCC-ee has in general the potential to constrain down to $\mathcal{O}(10^{-3} - 10^{-4})$ the ALP-photon-photon ($a\gamma\gamma$) and ALP-photon-dark-photon ($a\gamma\bar{\gamma}$) couplings, as defined in Eq. (1), assuming $\Lambda = 1$ TeV.

The diphoton+missing-energy signature we have proposed in this work not only shows a better signal-to-background ratio compared to the triphoton channel (for comparable couplings), but also provides an independent and stronger bounds on $C_{a\gamma\gamma}$ even for tiny but significant $C_{a\gamma\bar{\gamma}}$ (e.g., $C_{a\gamma\bar{\gamma}} \sim 10^{-3}$) compared to the case where $C_{a\gamma\bar{\gamma}} = 0$.

Note that our analysis is not sensitive to the CP property of the produced scalar particle, and can also be effectively used to probe possible couplings of CP-even scalars to photons and dark photons, if occurring in particular new physics scenarios.

The corresponding search strategies for the ILC, CLIC, CEPC collision-energy and integrated-luminosity setups can be inferred by the present analysis in a quite straightforward way.

ACKNOWLEDGMENTS

E. G. wish to thank the Theoretical Physics Department at CERN for its hospitality during the completion of this work. S. B. would like to thank the Korea Institute for Advanced Study for extending its hospitality while part of the work has been carried out and also thanks E. J. Chun for useful discussions and comments. A. C. would like to thank University Grant Commission, India, for supporting this work by means of a NET Fellowship (Ref. No. 22/06/2014 (i) EU-V and Sr. No. 2061451168).

[1] G. Aad *et al.* (ATLAS Collaboration), Phys. Lett. B **716**, 1 (2012); S. Chatrchyan *et al.* (CMS Collaboration), Phys. Lett. B **716**, 30 (2012).
[2] ATLAS Collaboration, CERN Report No. ATLAS-CONF-2019-005, 2019.
[3] A. M. Sirunyan *et al.* (CMS Collaboration), Eur. Phys. J. C **79**, 421 (2019).
[4] P. A. R. Ade *et al.* (Planck Collaboration), Astron. Astrophys. **571**, A16 (2014).
[5] For a review and references, see R. Essig *et al.*, arXiv: 1311.0029.
[6] E. Gabrielli and M. Raidal, Phys. Rev. D **89**, 015008 (2014).
[7] E. Gabrielli, L. Marzola, and M. Raidal, Phys. Rev. D **95**, 035005 (2017).
[8] B. Holdom, Phys. Lett. **166B**, 196 (1986).
[9] D. N. Spergel and P. J. Steinhardt, Phys. Rev. Lett. **84**, 3760 (2000).
[10] M. Vogelsberger, J. Zavala, and A. Loeb, Mon. Not. R. Astron. Soc. **423**, 3740 (2012).
[11] L. G. van den Aarssen, T. Bringmann, and C. Pfrommer, Phys. Rev. Lett. **109**, 231301 (2012).
[12] S. Tulin, H.-B. Yu, and K. M. Zurek, Phys. Rev. D **87**, 115007 (2013).
[13] L. Ackerman, M. R. Buckley, S. M. Carroll, and M. Kamionkowski, Phys. Rev. D **79**, 023519 (2009).

[14] J. Fan, A. Katz, L. Randall, and M. Reece, Phys. Rev. Lett. **110**, 211302 (2013).
[15] N. Arkani-Hamed, D. P. Finkbeiner, T. R. Slatyer, and N. Weiner, Phys. Rev. D **79**, 015014 (2009).
[16] K. M. Zurek, Phys. Rep. **537**, 91 (2014).
[17] R. D. Peccei and H. R. Quinn, Phys. Rev. Lett. **38**, 1440 (1977).
[18] E. Witten, Phys. Lett. B **149B**, 351 (1984).
[19] P. Svrcek and E. Witten, J. High Energy Phys. 06 (2006) 051.
[20] A. Arvanitaki, S. Dimopoulos, S. Dubovsky, N. Kaloper, and J. March-Russell, Phys. Rev. D **81**, 123530 (2010).
[21] B. S. Acharya, K. Bobkov, and P. Kumar, J. High Energy Phys. 11 (2010) 105.
[22] M. Bauer, M. Neubert, and A. Thamm, Phys. Rev. Lett. **119**, 031802 (2017).
[23] M. Bauer, M. Neubert, and A. Thamm, J. High Energy Phys. 12 (2017) 044.
[24] M. J. Dolan, T. Ferber, C. Hearty, F. Kahlhoefer, and K. Schmidt-Hoberg, J. High Energy Phys. 12 (2017) 094.
[25] I. Brivio, M. B. Gavela, L. Merlo, K. Mimasu, J. M. No, R. del Rey, and V. Sanz, Eur. Phys. J. C **77**, 572 (2017).
[26] K. Mimasu and V. Sanz, J. High Energy Phys. 06 (2015) 173.
[27] J. Jaeckel and M. Spannowsky, Phys. Lett. B **753**, 482 (2016).
[28] C. Baldenegro, S. Fichet, G. von Gersdorff, and C. Royon, J. High Energy Phys. 06 (2018) 131.
[29] J. Jaeckel and A. Ringwald, Annu. Rev. Nucl. Part. Sci. **60**, 405 (2010).
[30] J. Jaeckel, M. Jankowiak, and M. Spannowsky, Phys. Dark Universe **2**, 111 (2013).
[31] P. W. Graham, I. G. Irastorza, S. K. Lamoreaux, A. Lindner, and K. A. van Bibber, Annu. Rev. Nucl. Part. Sci. **65**, 485 (2015).
[32] L. Merlo, F. Pobbe, S. Rigolin, and O. Sumensari, J. High Energy Phys. 06 (2019) 091.
[33] P. Ilten, Y. Soreq, M. Williams, and W. Xue, J. High Energy Phys. 06 (2018) 004.
[34] M. Bauer, P. Foldenauer, and J. Jaeckel, J. High Energy Phys. 07 (2018) 094.
[35] K. Kaneta, H. S. Lee, and S. Yun, Phys. Rev. Lett. **118**, 101802 (2017).
[36] K. Kaneta, H. S. Lee, and S. Yun, Phys. Rev. D **95**, 115032 (2017).
[37] P. deNiverville, H. S. Lee, and M. S. Seo, Phys. Rev. D **98**, 115011 (2018).
[38] P. Bambade *et al.*, arXiv:1903.01629.
[39] P. N. Burrows *et al.* (CLICdp and CLIC Collaborations), *CERN Yellow Reports: Monographs* (CERN, Geneva, Switzerland, 2018), Vol. 18, p. 1.
[40] A. Abada *et al.* (FCC Collaboration), Eur. Phys. J. Spec. Top. **228**, 261 (2019).
[41] A. Abada *et al.* (FCC Collaboration), Eur. Phys. J. C **79**, 474 (2019).
[42] J. B. Guimares da Costa *et al.* (CEPC Study Group), arXiv:1811.10545.
[43] M. Banedikt, *Open Symposium—Update of the European Strategy for Particle Physics, Granada, Spain* (2019), https://cafpe.ugr.es/eppsu2019/.
[44] S. Davidson, B. Campbell, and D. C. Bailey, Phys. Rev. D **43**, 2314 (1991).
[45] G. G. Raffelt, *Stars as laboratories for fundamental physics: The astrophysics of neutrinos, axions, and other weakly interacting particles* (Chicago University Press, Chicago, 1996), p. 664.
[46] K. Kadota, T. Sekiguchi, and H. Tashiro, arXiv:1602.04009.
[47] S. Biswas, E. Gabrielli, M. Heikinheimo, and B. Mele, J. High Energy Phys. 06 (2015) 102; Phys. Rev. D **96**, 055012 (2017).
[48] J. Alwall, R. Frederix, S. Frixione, V. Hirschi, F. Maltoni, O. Mattelaer, H.-S. Shao, T. Stelzer, P. Torrielli, and M. Zaro, J. High Energy Phys. 07 (2014) 079.
[49] A. Alloul, N. D. Christensen, C. Degrande, C. Duhr, and B. Fuks, Comput. Phys. Commun. **185**, 2250 (2014).
[50] M. Gataullin (LEP Collaboration), Int. J. Mod. Phys. A **20**, 3273 (2005).